Phytoplankton contributions to the trace-element composition of Precambrian banded iron formations

Kurt O. Konhauser[1,†], Leslie J. Robbins[1], Daniel S. Alessi[1], Shannon L. Flynn[1], Murray K. Gingras[1], Raul E. Martinez[2], Andreas Kappler[3], Elizabeth D. Swanner[4], Yi-Liang Li[5], Sean A. Crowe[6], Noah J. Planavsky[7], Christopher T. Reinhard[8], and Stefan V. Lalonde[9]

[1]*Department of Earth and Atmospheric Sciences, University of Alberta, Edmonton, AB T6G 2E3, Canada*
[2]*Institut für Geo- und Umweltnaturwissenschaften, Albert-Ludwigs-Universität, Mineralogie-Geochemie, 79104 Freiburg, Germany*
[3]*Department of Geomicrobiology, Center for Applied Geosciences, University of Tübingen, 72074 Tübingen, Germany*
[4]*Department of Geological and Atmospheric Sciences, Iowa State University, Ames, Iowa 50011, USA*
[5]*Department of Earth Sciences, University of Hong Kong, Pokfulam Road, Hong Kong, China*
[6]*Department of Microbiology and Immunology and Department of Earth, Ocean, and Atmospheric Sciences, University of
 British Columbia, Vancouver, BC V6T 1Z4, Canada*
[7]*Department of Geology and Geophysics, Yale University, New Haven, Connecticut 06511, USA*
[8]*School of Earth and Atmospheric Sciences, Georgia Institute of Technology, Atlanta, Georgia 30332, USA*
[9]*European Institute for Marine Studies, CNRS-UMR6538 Laboratoire Domaines Océaniques, Technopôle Brest-Iroise, 29280
 Plouzané, France*

ABSTRACT

Banded iron formations are economically important sedimentary deposits in Earth's Precambrian rock record, consisting of alternating iron-rich (hematite, magnetite, and siderite) and silicate/carbonate (quartz, clay-like minerals, dolomite, and ankerite) layers. Based on chemical analyses from banded iron formation units of the 2.48 Ga Dales Gorge Member of the Hamersley Group in Western Australia, it has been previously suggested that most, if not all, of the iron in banded iron formations could have been oxidized by anoxygenic phototrophic bacteria (photoferrotrophs) at cell densities considerably less than those found in modern iron-rich aqueous environments. However, oxygen-producing phytoplankton may have also been capable of supplying the necessary oxidizing power. Here, we revisit the question of the anoxygenic and oxygenic phytoplankton populations necessary to account for banded iron formation deposition and quantify the amount of selected trace elements (P, Mn, Co, Ni, Cu, Zn, Mo, Cd) that could have been associated with their biomass. Using an expanded geochemical data set for the Dales Gorge Member as an example, we find that with turnover times comparable to those seen in modern ecosystems, the same phytoplankton populations required to form banded iron formations could have supplied the entirety of trace elements found in this iron-rich deposit. Further, spurred by the similarities between banded iron formation and anoxygenic phytoplankton trace-element stoichiometries, we suggest that much of the trace-element inventory preserved in the banded iron formation was at some point biologically assimilated in the water column, released from degrading photoferrotrophic biomass at the seafloor and in the sediment pile, and ultimately fixed in the iron-rich sediment in approximately stoichiometric proportions by near-quantitative adsorption to ferrihydrite. Our observations suggest that, as today, phytoplankton and the recycling of their biomass exerted control over the trace-element composition of ancient seawater and sediment.

INTRODUCTION

It is widely accepted that during the Precambrian, photosynthetic planktonic bacteria were involved in the oxidation of dissolved Fe(II) and the resultant precipitation of Fe(III), which led to banded iron formation deposition (for reviews, see Köhler et al., 2010; Posth et al., 2013). Two possible roles are envisioned. The first is predicated on the presence of ancient cyanobacteria (e.g., Cloud, 1973) that produced oxygen that reacted with dissolved Fe(II) to form ferric oxyhydroxide phases (e.g., Chan et al., 2016) such as ferrihydrite, $Fe(OH)_3$, the likely precursor sediment to banded iron formations (see Bekker et al., 2014; Konhauser et al., 2017). These oxygenic phototrophs would have flourished wherever bioessential trace elements were available, creating "oxygen oases" in the upper water column (Olson et al., 2013; Swanner et al., 2015), perhaps as early as 3.0 Ga (Crowe et al., 2013; Planavsky et al., 2014), if not earlier (see Satkoski et al., 2015; Frei et al., 2016). The second, and arguably the more ancient role, is ascribed to anoxygenic photosynthetic bacteria that used Fe(II) as a reductant for CO_2 fixation (e.g., Garrels and Perry, 1974; Ehrenreich and Widdel, 1994). Although the Fe(II) oxidation rate of these photoferrotrophs is dependent upon light intensity, they can grow in low-light regimes befitting the deeper marine photic zones (e.g., Biebl and Pfennig, 1978; Crowe et al., 2008); it has been estimated that sufficient light for their metabolism could penetrate up to 100 m ocean depth (Kappler et al., 2005). Therefore, these microorganisms could easily have oxidized all the upwelling Fe(II) before it met oxygenated surface waters (if these existed) in Archean oceans. Moreover, Jones et al. (2015) recently suggested that photoferrotrophs could also have exhausted dissolved phosphorous in upwelling

[†]kurtk@ualberta.ca

waters, depriving cyanobacteria in overlying waters of this key nutrient.

Over a decade ago, Konhauser et al. (2002) calculated that for a major banded iron formation deposit, such as the 2.48 Ga Dales Gorge Member of the Brockman Iron Formation, Hamersley Group, Western Australia, on average 4.53×10^{12} moles of Fe (or 45.3 mol m^{-2} when normalized to a surface area of 10^{11} m^2) were precipitated annually during periods of peak ferric iron deposition. This sedimentation rate would have required some 5.0×10^{23} cells of either photoferrotrophic (e.g., *Chromatium* sp.) or microaerophilic, chemolithoautotrophic, Fe(II)-oxidizing bacteria (e.g., *Gallionella* sp.) per year. Assuming that Fe(II) oxidation was restricted to the upper 100 m of the water column, then a minimum cell density of ~5×10^4 cells mL^{-1} would have been required to precipitate an annual banded iron formation layer (Konhauser et al., 2002). Once the phytoplankton died, some of the cellular remains would have settled through the water column with ferrihydrite particles and been deposited at the seafloor as the precursor sediment to the banded iron formation. These biomass-ferrihydrite aggregates then would have served as substrata for bacteria performing dissimilatory Fe(III) reduction (DIR) within the sediments, leading to the oxidation (and loss) of organic carbon, as well as the early diagenetic precipitation of Fe(II)-bearing minerals, such as magnetite (Fe_3O_4) and siderite ($FeCO_3$; e.g., Konhauser et al., 2005; Heimann et al., 2010; Li et al., 2011; Köhler et al., 2013). At the time, Konhauser et al. (2002) speculated that those ferrihydrite particles undergoing sedimentation would have transported trace elements to the seafloor along with the decaying biomass. However, several recent studies have since suggested that in the Precambrian oceans, those same minerals may not have been as reactive as previously believed because dissolved silica (e.g., Konhauser et al., 2007a, 2009; Jones et al., 2015) and organic carbon (Eickhoff et al., 2014) passivate the surface reactivity of ferrihydrite toward other ions.

It is also possible that the biomass itself may have been a major contributor to the trace-element inventory of banded iron formations. Li et al. (2011) suggested that phytoplankton may have played a key role in the transfer of phosphorous (via intracellular assimilation) from the photic zone to the seafloor. It is also likely that marine phytoplankton, having high surface reactivity (e.g., Sañudo-Wilhelmy et al., 2004; Dittrich and Sibler, 2005; Hadjoudja et al., 2010; Liu et al., 2015), could similarly have adsorbed cationic trace metals, and ultimately facilitated their deposition into marine sediments such as banded iron formations. Indeed, Martinez et al.

(2016) recently applied surface complexation modeling (SCM) to describe trace-metal cation adsorption to one of the two marine photoferrotrophs isolated to date, *Rhodovulum iodosum* (the other being *Rhodovulum robiginosum*; Straub et al., 1999), and calculated that the trace-metal inventory (i.e., Mn, Co, Cu, Zn, Ni, and Cd) in the 3.75 Ga banded iron formation in the Nuvvuagittuq Supracrustal Belt in Quebec, Canada, could entirely be accounted for by adsorption onto bacterial surface functional groups at ocean-relevant aqueous conditions. Importantly, Hao et al. (2013) and Martinez et al. (2016) also determined that in the composites of ferrihydrite, intact cells, and extracellular polysaccharides (EPS) produced by photoferrotrophs, the surface functional groups responsible for most of the metal cation adsorption were those corresponding to the organic matter fraction. This is consistent with the results of previous studies of bacteriogenic iron-oxide surface reactivity, where the surface charge of such organic-mineral composites was dominated by contributions from reactive groups associated with the bacterial cell fraction (Mikutta et al., 2012; Moon and Peacock, 2013). Similarly, Liu et al. (2015) evaluated Cd adsorption onto the marine cyanobacterium *Synechococcus* sp. PCC 7002 and demonstrated that an active bloom with 10^4–10^5 cells/mL at pH 8 could adsorb 1–10 nmol of Cd per liter of seawater. Indeed, at a total Cd concentration in modern seawater of 8 n*M* (e.g., Pai and Chen, 1994), a population of *Synechococcus* could theoretically adsorb nearly all dissolved Cd from seawater in the photic zone if equilibrium metal adsorption conditions were achieved. Of course, near-complete Cd adsorption to marine biomass is not observed due to competing adsorption reactions, as well as aqueous Cd complexation in seawater by chloride (predominantly as $CdCl_2^0$ and $CdCl^+$; Byrne et al., 1988) and by organic ligands (Bruland, 1992), all of which act to reduce the concentration of free aqueous Cd^{2+} available to adsorb to cell surface functional groups.

In this study, we revisited the quantity of trace elements supplied by biomass to banded iron formations. We first estimated the amount of ferric iron deposited in an annual layer and, in turn, the amount of trace elements deposited annually, using literature and new geochemical data obtained for the Dales Gorge Member. For photoferrotrophic biomass, refined surface adsorption models have recently become available (Martinez et al., 2016), which allow for an evaluation of the amount of trace elements that could have been sequestered through adsorption. To date, high-quality trace-element assimilation data for photoferrotrophs are lacking, and therefore, we performed a series of experiments to provide per-

cell metal loadings associated with their biomass. As a comparison, we also considered per-cell metal loadings associated with metal assimilation by oxygen-evolving cyanobacterial and eukaryotic phytoplankton. The expected flux of trace metals from these different biomass sources to banded iron formations was then evaluated in light of both the number of phytoplankton cells implicated in banded iron formation deposition (i.e., only enough cells to form the banded iron formation), and more realistic cell numbers when modern turnover rates are considered, in order to understand their contribution to banded iron formation trace-element inventories.

METHODS

Banded Iron Formation Trace-Metal Analyses

To assess the importance of biomass as a trace-metal shuttle to banded iron formation sediment, we first assembled an expanded trace-metal data set for the 2.48 Ga Dales Gorge Member, the banded iron formation from which Konhauser et al. (2002) made the initial calculations on the number of bacteria that would be required annually to precipitate the ferric iron component in the banded iron formation. Data were sourced from literature, as well as new geochemical analyses of recently obtained drill core samples (Table S1 in the GSA Data Repository[1]). In this work, we focused on banded iron formation oxide facies (rich in hematite and magnetite; cf. James, 1954) because it is generally presumed that they formed via dehydration and/or partial reduction of a precursor ferrihydrite phase (Ewers and Morris, 1981; Han, 1988; Ahn and Buseck, 1990; Krapež et al., 2003; Bekker et al., 2010) and thus contain the most "primary" iron minerals in the banded iron formation (Huberty et al., 2012; Li et al., 2013; Sun et al., 2015). An alternative interpretation proposing that greenalite ($Fe_3Si_2O_5[OH]_4$) was the primary phase, and was oxidized by oxygen-bearing meteoric waters sometime after 2.2 Ga, has been advanced (see Rasmussen et al., 2015, 2016, 2017), but this view is inconsistent with iron isotope data (e.g., Johnson et al., 2008a; Planavsky et al., 2012).

For new trace-element analyses performed for this study, samples were cut into slabs and broken into small chips (<5 mm) without metal contact, and between 20 and 150 g aliquots

were powdered in an automated agate mill. Approximately 50 mg aliquots of crushed rock powder (<100 mesh) were digested sequentially in a class 1000 clean laboratory at the Institut Français de Recherche pour l'Exploitation de la Mer (IFREMER), Centre de Brest, France, in perfluoroalkoxy (PFA) vials at 90 °C using concentrated HF-HNO$_3$, aqua regia, and 6 M HCl. Aliquots were resuspended in 2% HNO$_3$ with indium as an internal standard and analyzed for trace-element concentrations using a Thermo Scientific Element2 high-resolution inductively coupled plasma–mass spectrometer (ICP-MS) at the Pôle Spectrométrie Océan in Brest, France. The instrument was calibrated with multi-element solutions, and the results were verified against geostandards BHVO-2, IF-G, and GL-O treated in the same batch. Precisions based on the repeated analysis of standards, expressed as 2 relative standard deviations (RSD), ranged from <3% for rare earth elements analyzed at low resolution to 4%–8% for transition metals analyzed at medium resolution.

Growth of *R. iodosum*

The basal salts and NaHCO$_3$ of marine phototroph (MP) medium for the cultivation of *R. iodosum* were prepared according to the protocol described by Wu et al. (2014). Sterile additions made after autoclaving included 3 mg L^{-1} filtered FeCl$_3$, a selenium and tungstate solution (0.4 g NaOH, 6 mg Na$_2$SeO$_3$•5H$_2$O, and 8 mg Na$_2$WO$_4$•2H$_2$O in 1 L Millipore water), 0.5 mM Na$_2$S$_2$O$_3$, and 1 mL each of a vitamin and trace-element solution. For the trace-element solution, 5 mL aliquots of 25% HCl were added to 495 mL of ultrapure water containing 2.9 g L^{-1} H$_3$BO$_3$, 0.5 g L^{-1} MnCl$_2$·4H$_2$O, 24 mg L^{-1} NiCl$_2$·6H$_2$O, 190 mg L^{-1} CoCl$_2$·6H$_2$O, 180 mg L^{-1} ZnCl$_2$, 36 mg L^{-1} Na$_2$MoO$_4$·2H$_2$O, 2 mg L^{-1} CuCl$_2$·2H$_2$O, and a final concentration of 7.5 mM Fe(II) added from an oxidized elemental Fe solution to eliminate trace-metal contamination from using an Fe(II) salt. The elemental Fe was washed with acetone to remove organic contaminants and then dissolved and oxidized to Fe(II) in anoxic 1 N HCl in a glovebox (100% N$_2$). The vitamin solution contained 10 mg L^{-1} D(+)-biotin, 50 mg L^{-1} vitamin B$_1$, 250 mg L^{-1} vitamin B$_6$, 50 mg L^{-1} aminobenzoic acid, 25 mg L^{-1} D-pantothenic acid, 100 mg L^{-1} nicotinic acid, and 1 g L^{-1} vitamin B$_{12}$. The pH of the medium was adjusted to 6.8 using 1 N HCl or 0.5 M Na$_2$CO$_3$ as described in Hegler et al. (2008). To determine how the photoferrotrophs responded to varying concentrations of metals, we varied the amount of metal in the medium by adding trace-element solutions representing 0.5×, 1×, 2×, and 5× the metal concentrations in the basal

(1×) medium. The concentration of metals in the 1× medium was as follows (in μM): V (0.03), Mn (2.30), Co (1.2), Ni (0.23), Cu (0.05), Zn (2.42), Mo (0.27), and Cd (0.00007).

Samples of media (100 mL) were dispensed into 200 mL borosilicate glass bottles and sealed with butyl rubber stoppers to maintain anoxic conditions. All glassware was of borosilicate composition and was acid-washed in 1 N HCl for 24 h, then soaked in ultrapure water (conductivity 0.0555 μS) for at least 48 h, and then rinsed with fresh ultrapure water to remove adsorbed metals. Butyl rubber stoppers were acid-washed in 1 N HCl for 24 h and then boiled three times in ultrapure water.

Experiments were inoculated to 1% (v/v) with a log-phase culture. All experiments were conducted in triplicate. Cultures of *R. iodosum* were incubated at a constant intensity of 12.82 μmol photons m^{-2} s^{-1} from a standard 40 W tungsten light bulb at 24 °C under static conditions.

Metal Assimilation by *R. iodosum*

The concentrations of all metals in trace-element and vitamin solutions were determined using an inductively coupled plasma–optical emission spectrometer (ICP-OES; Perkin Elmer Optima 5300 or Horiba Ultima 2) or ICP-MS (Thermo Scientific Element2). Certified commercial multi-element standards were used for calibration. Liquid samples of all media depleted in metals were analyzed in triplicate. To determine the concentration of metals in the cytoplasm, cells were harvested in the stationary phase by centrifugation, and the pellet was washed three times in 0.01 N HCl to remove adsorbed metals from the cell surface. The cells were freeze-dried and then digested in concentrated trace-metal-grade HNO$_3$ at 60 °C in acid-washed PFA vials. The residues were resuspended in 8 M HNO$_3$ and further diluted in 2% HNO$_3$ before analysis.

The concentrations of metals in dried biomass were used to determine the cellular metal quotas (Q_{Me}; μmoles L^{-1}) present in cells under different conditions. The number of cells per liter was determined after establishing a standard curve relating OD$_{660}$ (optical density at a wavelength of 660 nm) measurements to fluorescent cell counts (Wu et al., 2014). Then, a suspension of a known cell density was dried and weighed to determine the dried biomass weight.

Modeling Bacterial Surface Reactivity to Various Divalent Cations

Martinez et al. (2016) recently investigated the surface proton reactivity of a *R. iodosum*–

ferrihydrite composite and calculated protonation constants (pK_a values) and corresponding site densities. Using the protonation model of Martinez et al. (2016), we employed a free linear energy approach to extrapolate metal-organic binding constants from metal-acetate complexes (constants from Martell and Smith, 1977) to cell surface carboxyl groups (cf. Fein et al., 2001; Martinez et al., 2016). This is justified because carboxyl groups are the dominant deprotonated sites for metal adsorption at marine pH values, and bacteria have been repeatedly shown to exhibit broadly similar metal-binding behavior across species (e.g., Yee and Fein, 2001; Borrok et al., 2004a, 2004b). We employed a modern seawater pH of 8 for all adsorption calculations, consistent with previously predicted ranges for Paleoproterozoic seawater (e.g., 5.7–8.3 *in* Grotzinger and Kasting, 1993; 7.7–8.3 *in* Tosca et al., 2016; 6.7–7.8 *in* Blättler et al., 2017). Additional constraints included *R. iodosum* cell densities of 1.9×10^4 cells/mL (see following), and an initial trace-metal composition equivalent to modern mean seawater, after Bruland and Lohan (2003).

To calculate the removal of trace metals from seawater to *R. iodosum* surface functional groups, we first determined the number of deprotonated ligands at pH 8 using the protonation model of Martinez et al. (2016). Then, using metal binding constants calculated as described above, we calculated the concentration of metal removed from solution, for each metal individually. The concentration of deprotonated bacterial surface sites (mol sites/L seawater), was nearly three times greater than the sum concentration of all trace metals of interest. Following adsorption, only a miniscule fraction, well under 0.1%, of the total deprotonated sites is occupied by the tested metals. For this reason, a model that considered the simultaneous competition of all tested metals for adsorption to *R. iodosum* surface sites was deemed unnecessary.

Model runs were performed for three versions of seawater, one with a modern composition (after Bruland and Lohan, 2003), one simulating the composition of seawater during deposition of the 2.48 Ga Dales Gorge Member, and one stoichiometrically fixed to *R. iodosum* and 9 nM Ni (Table S2 [see footnote 1]). Simulated Paleoproterozoic seawater was set at 10 nM Co, 3 nM Cu, 400 nM Ni, 10 nM Zn, and 0.6 nM Cd and was based on upper estimates for several trace metals to test conditions under which the greatest extent of metal competition and adsorption is expected. Estimates were derived from empirical rock record constraints when possible (Ni, Zn), or from thermodynamic solubility limits when those were unavailable (Mn). Zn was set at 10 nM based

on Robbins et al. (2013) and Scott et al. (2013); similarly, Ni was set at 400 n*M* based on Konhauser et al. (2009, 2015). For Cu, a modern concentration was assumed, because the geological record shows little variation (Fru et al., 2016). Manganese was increased to above modern values based on the estimates of Saito et al. (2003). Finally, Co was set at a higher concentration than modern based on Saito et al. (2003) and Swanner et al. (2014). Because of the lack of strong empirical constraints, Cd was maintained at modern concentrations.

Modeling Metal Adsorption by Ferrihydrite

The adsorption of trace metals to ferrihydrite was modeled using the chemical speciation software Visual MINTEQ (Gustafsson, 2013) and the hydrous ferric oxide (HFO) surface complexation model of Dzombak and Morel (1990), which is built into the Visual MINTEQ package. This model invokes two amphoteric functional groups at the HFO surface to account for proton and metal adsorption and a diffuse double layer to account for the electrostatic field that develops as a function of pH and ionic strength at the HFO surface. Modeling conditions were 25 °C with a matrix of 0.56 *M* NaCl. Metals were allowed to simultaneously compete for adsorption onto surface sites, and we accounted for the impacts of major hydroxide, carbonate, and chloride aqueous complexes with the metals of interest. To evaluate how trace elements released from decaying biomass may be fractionated during adsorption to ferrihydrite, adsorption was calculated using the trace-metal composition of simulated seawater with the trace metals under consideration fixed to phototrophic assimilated proportions, anchored around a fixed Ni concentration of 9 n*M*, similar to modern seawater and conservatively below estimates for Paleoproterozoic seawater ca. 2.48 Ga (Konhauser et al., 2009; Table S2 [see footnote 1]; see also following discussion).

RESULTS AND DISCUSSION

Amount of Trace Elements in an Annual Banded Iron Formation Layer

In Konhauser et al. (2002), the authors purposefully used a sedimentation rate of 1 mm yr^{-1} hematite equivalent (assuming ~95% compaction, where the actual wet sediment deposition rate would have been much higher; Trendall and Blockley, 1970) throughout the Hamersley Basin (10^{11} m^2) to emphasize that even under unrealistically rapid sedimentation rates, marine bacteria could have precipitated all the ferric iron in the Dales Gorge Member banded iron formation. In this study, we conservatively applied lower sedimentation rates based on a proposed modern analogue for banded iron formation deposition, the ferruginous Lake Matano in Indonesia (Crowe et al., 2008). By measuring a sedimentation rate of 0.8 mm yr^{-1}, a sedimentary Fe content of 20 wt%, a sediment water content of 90% by mass, and a particle density of 2.97×10^6 g m^{-3}, Crowe et al. (2011) determined an Fe burial rate of 8.5×10^{-3} mol m^{-2} d^{-1}. Kuntz et al. (2015) subsequently recalculated the total iron fluxes in Lake Matano as 1.86×10^{-3} mol m^{-2} d^{-1}, using the following equation: $R_{Fe} = R_{sed}(1 - \theta)(\rho_{sed})(wt\%_{Fe})(1/M_{Fe})$. While this Fe burial flux both contains a detrital component and is influenced by the hydrodynamics of Lake Matano, neither of which are strongly analogous to the Precambrian marine systems, these observations demonstrate that appreciable Fe burial is possible under anoxic ferruginous conditions. They thus provide a real-world benchmark against which modeled banded iron formation burial fluxes can be compared.

For the Dales Gorge Member, considering a presumed initial deposit of 80 wt% Fe(OH)$_3$ (equivalent to 42 wt% Fe) and 20 wt% amorphous SiO$_2$ (which is now manifest as Fe-rich mesobands in oxide-type banded iron formation layers containing ~80% hematite/magnetite and 20% quartz; Konhauser et al., 2002), with corresponding densities of 3.8 g cm^{-3} and 2.2 g cm^{-3}, respectively, yielding a total density of 3.48×10^6 g m^{-3}, the estimated sedimentation rate might have been as low as 0.3 mm yr^{-1}. At this sedimentation rate over the entire depositional area of 10^{11} m^2, the annual Dales Gorge banded iron formation mass would have been 1.04×10^{11} kg. We further note that the assumption of a 20% initial silica component for the ferrihydrite particles undergoing sedimentation is consistent with recent studies that have suggested that the primary Fe(III) precipitate in banded iron formations was an Fe(III)–silica gel (Percak-Dennett et al., 2011; Reddy et al., 2016; Zheng et al., 2016).

Based on geochemical analyses of banded iron formation oxide facies in the Dales Gorge Member (Alibert and McCulloch, 1993; Pecoits et al., 2009; Konhauser et al., 2009, 2011), as well as new analyses performed for this study (see Table S1), we calculated average concentrations (in mg kg^{-1}) for P (859.40), Zn (13.12), Co (3.90), Cu (4.18), Ni (4.50), Mo (1.24), Cd (1.21), and Mn (228.63). Using the annual mass calculated earlier herein, this translates into an average annual flux (in mol yr^{-1}; see Table 1A) of P (2.90×10^9), Zn (2.10×10^7), Co (6.91×10^6), Cu (6.87×10^6), Ni (8.00×10^6), Mo (1.35×10^6), Cd (1.12×10^6), and Mn (4.34×10^8).

Number of Cells Required to Form an Annual Banded Iron Formation Layer

Peak iron deposition in the Dales Gorge Member is estimated at 4.38×10^{13} g or 7.85×10^{11} mol of Fe yr^{-1} (based on the mass calculation of 1.04×10^{11} kg and an average Fe$_{TOTAL}$ of 42 wt% for the precursor sediments). For oxygen-evolving phytoplankton (e.g., cyanobacteria) to have been responsible for Fe(II) oxidation (using $12Fe^{2+} + 3O_2 + 30H_2O \rightarrow 12Fe(OH)_3 + 24H^+$), a net oxygen production rate of ~1.96×10^{11} mol O$_2$ yr^{-1} would have been needed. For the Dales Gorge Member depositional basin estimated at 10^{11} m^2, this translates to a depth-integrated production rate of 5.37 mmol O$_2$ m^{-2} d^{-1}. Depth-integrated net oxygen production rates in modern ocean regions generally range from slightly below zero (net heterotrophic; Arabian Sea, North Pacific Gyre) to 10–40 mmol O$_2$ m^{-2} d^{-1} (NE Atlantic, Mediterranean Sea, Baltic Sea), with highly productive regions like the Southern Ocean reaching up to ~110 mmol O$_2$ m^{-2} d^{-1} (Williams, 1998). Cyanobacteria in the Hamersley Basin photic zone would thus need to achieve net O$_2$ production rates that are at the lower end of what is observed today. Assuming a 100 m photic zone and a cyanobacteria cell-specific O$_2$ production rate of 50 fmol cell^{-1} h^{-1} (Tang et al., 2014), this translates to a total population of 4.5×10^{20} cells, or only ~45 cells mL^{-1}, needed to form banded iron formation. This cell density is unrealistically low, considering that it assumes a maximal rate of oxygen production under optimal light and nutrient conditions in culture (Tang et al., 2014), but it is important nonetheless in that it quantitatively demonstrates for the first time that relatively small populations of cyanobacteria could readily have generated the oxidizing equivalents required for banded iron formation deposition. Interestingly, the modest depth-integrated O$_2$ production rate required to oxidize the Fe(II) in the Dales Gorge Member (5.37 mmol O$_2$ m^{-2} d^{-1}) means that even muted photic zone O$_2$ production (by modern standards) would have had the effect of completely scrubbing dissolved Fe(II) from seawater, such that the upper photic zone in the Paleoproterozoic (and thereafter) would have had essentially no dissolved Fe(II).

In the case of photoferrotrophy, instead of using the cell densities from Konhauser et al. (2002), who calculated the cell number–normalized Fe(II) oxidation rates for the freshwater *Chromatium* sp. strain L7 (as per Ehrenreich and Widdel, 1994), we use here the recently determined Fe(II) oxidation rates for the marine strain *R. iodosum*. Based on reported Fe(II) oxidation rates of 0.15 m*M* Fe(II) d^{-1} at 0.43 m*M* Fe(II), a light intensity of 12 μmol photons m^{-2} s^{-1},

TABLE 1. TRACE METALS ASSOCIATED WITH BANDED IRON FORMATION LAYERS AND VARIOUS PHYTOPLANKTON

	P	Zn	Co	Cu	Ni	Mo	Cd	Mn
(A) Fe-rich mesoband composition								
Maximum concentration (mg kg^{-1})	11601.64	325.87	69.19	48.52	47.58	4.62	3.35	6331.73
Average concentration (mg kg^{-1})	859.40	13.12	3.90	4.18	4.50	1.24	1.21	228.63
Minimum concentration (mg kg^{-1})	1.22	0.18	0.21	0.03	0.34	0.09	0.06	0.08
Mesoband mass/yr (kg)	1.04E+11	1.04E+11	1.04E+11	1.04E+11	1.04E+11	1.04E+11	1.04E+11	1.04E+11
Molecular mass (mg mol^{-1})	30974	65380	58933	63546	58693	95960	112410	54938
Maximum amount in BIF layer (mol yr^{-1})	3.91E+10	5.20E+08	1.23E+08	7.97E+07	8.46E+07	5.03E+06	3.11E+06	1.20E+10
Average amount in BIF layer (mol yr^{-1})	2.90E+09	2.10E+07	6.91E+06	6.87E+06	8.00E+06	1.35E+06	1.12E+06	4.34E+08
Minimum amount in BIF layer (mol yr^{-1})	4.11E+06	2.91E+05	3.68E+05	4.76E+04	6.05E+05	9.47E+04	5.76E+04	1.58E+05
(B) *Rhodovulum*—assimilation								
Cell volume (μm^3)*	1.5	1.5	1.5	1.5	1.5	1.5	1.5	1.5
Cell mass (g)[†]	1.50E−12	1.50E−12	1.50E−12	1.50E−12	1.50E−12	1.50E−12	1.50E−12	1.50E−12
Cell requirements ($\mu g\ g^{-1}$)	25991.58	352.16	30.81	20.12	36.33	4.79	0.02	45.49
Single-cell concentration (μg)	3.90E−08	5.28E−10	4.62E−11	3.02E−11	5.45E−11	7.19E−12	3.00E−14	6.82E−11
Single-cell concentration (mol)	1.26E−15	8.08E−18	7.84E−19	4.75E−19	9.28E−19	7.49E−20	2.67E−22	1.24E−18
Normalized to P x1000	1000.00	6.41	0.62	0.38	0.74	0.06	0.0002	0.99
Minimum number of cells needed to form BIF	1.91E+23	1.91E+23	1.91E+23	1.91E+23	1.91E+23	1.91E+23	1.91E+23	1.91E+23
Annual biomass requirement (mol yr^{-1})	2.40E+08	1.54E+06	1.50E+05	9.07E+04	1.77E+05	1.43E+04	5.10E+01	2.37E+05
(C) *Rhodovulum*—adsorption[§]								
Total biomass needed to form BIF (mg)	2.87E+14	2.87E+14	2.87E+14	2.87E+14	2.87E+14	2.87E+14	2.87E+14	2.87E+14
Surface adsorption from modern seawater ($\mu mol\ mg^{-1}$ biomass)[#]	n.d.	5.03E−06	2.01E−08	2.73E−05	2.72E−06	n.d.	2.42E−06	1.22E−07
Surface adsorption (mol) per cell	n.d.	7.55E−21	3.02E−23	4.10E−20	4.08E−21	n.d.	3.63E−21	1.83E−22
Annual biomass requirement at [seawater] (mol yr^{-1})	n.d.	1.44E+03	5.77E+00	7.82E+03	7.79E+02	n.d.	6.93E+02	3.50E+01
(D) Total metals with photoferrotrophs								
Single-concentration (mol) assimilated+adsorbed	1.26E−15	8.09E−18	7.84E−19	5.16E−19	9.33E−19	7.49E−20	3.90E−21	1.24E−18
Annual biomass contribution (mol yr^{-1})	2.40E+08	1.54E+06	1.50E+05	9.85E+04	1.78E+05	1.43E+04	7.44E+02	2.37E+05
Relative to BIF	0.0830	0.0737	0.0217	0.0143	0.0223	0.0106	0.0007	0.0005
Total cells for 3 d doubling time	2.31E+25	2.31E+25	2.31E+25	2.31E+25	2.31E+25	2.31E+25	2.31E+25	2.31E+25
Annual biomass contribution (mol yr^{-1})	2.91E+10	1.87E+08	1.81E+07	1.19E+07	2.16E+07	1.73E+06	9.00E+04	2.87E+07
Relative to BIF	10.04	8.92	2.62	1.74	2.69	1.28	0.08	0.07
(E) Average marine cyanobacteria								
Single-cell metal quantity (mol cell^{-1})**	1.51E−16	2.48E−19	3.28E−21	6.34E−20	2.92E−19	7.38E−20	1.08E−21	1.90E−19
Total cells at 4.5×10^1 cells mL^{-1}	4.50E+20	4.50E+20	4.50E+20	4.50E+20	4.50E+20	4.50E+20	4.50E+20	4.50E+20
Annual biomass contribution (mol yr^{-1})	6.78E+04	1.12E+02	1.47E+00	2.86E+01	1.31E+02	3.32E+01	4.86E−01	8.55E+01
Relative to BIF	2.34E−05	5.33E−06	2.13E−07	4.16E−06	1.64E−05	2.46E−05	4.33E−07	1.97E−07
Total cells for 3 d doubling time	5.45E+22	5.45E+22	5.45E+22	5.45E+22	5.45E+22	5.45E+22	5.45E+22	5.45E+22
Annual biomass contribution (mol yr^{-1})	8.20E+06	1.35E+04	1.78E+02	3.45E+03	1.59E+04	4.02E+03	5.88E+01	1.03E+04
Relative to BIF	2.83E−03	6.45E−04	2.58E−05	5.03E−04	1.98E−03	2.98E−03	5.23E−05	2.38E−05
(F) Ferrihydrite—adsorption from seawater with photoferrotroph-like trace-element composition[††]								
Moles adsorbed/mol Fe at 5 ppm Fe	4.35E−02	1.15E−03	9.68E−06	8.34E−04	5.38E−05	2.49E−10	1.00E−08	9.68E−06
Moles adsorbed/mol Fe at 500 ppm Fe	3.98E−03	1.42E−04	6.48E−06	9.94E−06	1.43E−05	5.89E−10	1.13E−08	8.22E−06
Moles adsorbed/mol Fe at 5000 ppm Fe	4.08E−04	1.56E−05	1.45E−06	9.96E−07	1.79E−06	9.88E−08	6.49E−09	2.27E−06
Moles of Fe(III) deposited annually	7.85E+11	7.85E+11	7.85E+11	7.85E+11	7.85E+11	7.85E+11	7.85E+11	7.85E+11
Annual ferrihydrite contribution at 5 ppm Fe (mol yr^{-1})	3.41E+10	9.03E+08	7.60E+06	6.55E+08	4.22E+07	1.95E+02	7.85E+03	7.60E+06
Annual ferrihydrite contribution at 500 ppm Fe (mol yr^{-1})	3.12E+09	1.11E+08	5.08E+06	7.81E+06	1.12E+07	4.63E+02	8.87E+03	6.45E+06
Annual ferrihydrite contribution at 5000 ppm Fe (mol yr^{-1})	3.20E+08	1.22E+07	1.14E+06	7.82E+05	1.40E+06	7.76E+04	5.10E+03	1.78E+06

Note: n.d.—not determined; BIF—banded iron formation.
*Straub et al. (1999).
[†]Hallbeck and Pedersen (1991).
[§]This work (see methods), using constants from Martinez et al. (2016).
[#]Mean seawater concentration from Bruland and Lohan (2003).
**Trace-element data from Walve et al. (2014).
[††]This work, calculated using Visual MINTEQ (see Methods).

and a cell density of 2.3×10^8 cells mL^{-1} during logarithmic growth phase at 240 h, Wu et al. (2014) calculated that each individual cell (taking day-night light cycles into consideration) can oxidize 4.11×10^{-12} moles Fe(II) yr^{-1}. At an annual precipitation rate of 7.85×10^{11} mol of Fe, ~1.91×10^{23} metabolizing cells of *R. iodosum* would be required to precipitate an annual banded iron formation layer. Taking the same depositional basin area and 100 m photic zone as above, this yields a minimum cell density of 1.91×10^4 cells mL^{-1}. This is approximately one third of the cell density required by the calculations of Konhauser et al. (2002) for banded iron forma-

tion deposition (having then assumed 1 mm yr^{-1} deposition of hematite) by *Chromatium* sp. strain L7, effectively validating those earlier calculations with data from a second strain. The importance of these calculations is that the cell densities necessary to precipitate the ferric iron in banded iron formations are considerably less than modern populations of bacterial phytoplankton growing in the photic zone of modern marine coastal waters (10^4–10^6 cells mL^{-1}; Miyazono et al., 1992; Jacquet et al., 1998).

We emphasize that these calculations correspond to the minimum number of cells required to precipitate banded iron formation layers, not the

maximum carrying capacity of the water column. They also disregard cell turnover, which is an important factor when considering the total amounts of metals that would have been associated with sinking biomass over the course of banded iron formation deposition (see following). Finally, these calculations ignore the possibility of alternative oxidation mechanisms, such as ultraviolet (UV) photo-oxidation, or atmosphere-derived oxidants, such as hydrogen peroxide; however, several studies suggest these mechanisms are of less importance than the biological oxidation mechanisms we explore here (e.g., Konhauser et al., 2007b; Pecoits et al., 2015).

Potential Contributions from Trace Elements Assimilated by Photoferrotrophic Biomass

In terms of trace-element assimilation, we determined that a population of *R. iodosum* cells at stationary phase incorporated from the 1× medium the following (average in µg g^{-1}): P (25992), Zn (352.2), Co (30.8), Cu (20.1), Ni (36.3), Mo (4.8), Cd (0.02), and Mn (45.5). Growth rates for *R. iodosum* did not change significantly between the 1× and 0.5×, 2×, or 5× metals media (Table S3 [see footnote 1]). Biomass yields were significantly higher in the 0.5× medium as compared to 1×, and lower in the 5× medium as compared to 1×, while the range of intracellular metal concentrations varied little despite changes in the medium composition.

Although elemental variability naturally occurs between species as a function of growth rate and in response to ambient nutrient concentrations in seawater (Bruland et al., 1991; Twining et al., 2004), and it is possible that ancestral photoferrotrophs may have behaved differently, the intracellular metal concentrations we determined for *R. iodosum* provide a basis for examining the magnitude of the rate at which phytoplankton may assimilate trace elements from seawater. To start, we first estimated the mass of an individual *R. iodosum* cell as follows: With an average *R. iodosum* cell volume of 1.5 µm^3 (Straub et al., 1999), and a proportionate mass to *Gallionella* (where each cell has a volume of ~1 µm^3 and has a wet mass of 1×10^{-12} g; Hallbeck and Pedersen, 1991), an individual *R. iodosum* cell is 1.5×10^{-12} g cell^{-1}. Then, using our elemental stoichiometry from above, we calculated the mass of trace elements assimilated by an individual *R. iodosum* cell, which, multiplied by a total cell population of 1.91×10^{23} cells, yields an annual quantity assimilated (in mol yr^{-1}) for the entire 100-m-deep photic zone for P (2.40×10^8), Zn (1.54×10^6), Co (1.50×10^5), Cu (9.07×10^4), Ni (1.77×10^5), Mo (1.43×10^4), Cd (5.10×10^1), and Mn (2.37×10^5) (Table 1B).

## Quantity of Trace Elements Adsorbed by *R. Iodosum*

Using the calculated adsorption values for *R. iodosum* (methods above; Table S4 [see footnote 1]), we calculated the amounts of metal adsorbed for modern mean seawater concentrations (Bruland and Lohan, 2003) at pH 8 (in µmol of metal mg^{-1}) as follows: Zn (5.03×10^{-6}), Co (2.01×10^{-8}), Cu (2.73×10^{-5}), Ni (2.72×10^{-6}), Cd (2.42×10^{-6}), and Mn (1.22×10^{-7}). For a photoferrotroph population of 1.91×10^{23} cells, each at an estimated 1.5×10^{-12} g cell^{-1}, this equates to annual fluxes due to biomass adsorption (in mol yr^{-1}):

Zn (1.44×10^3), Co (5.77), Cu (7.82×10^3), Ni (7.79×10^2), Cd (6.93×10^2), and Mn (3.50×10^1) (see Table 1C). Importantly, for most elements analyzed, we calculated that intracellular assimilation of metals accounts for between one to four orders of magnitude more metal than does adsorption to surface functional groups at seawater conditions (Table 1D). Accordingly, we consider assimilation to be the more important mechanism for the concentration of metals by *R. iodosum* biomass. Cd, which is a notable exception, likely has a more restricted role in metalloenzymes (e.g., Price and Morel, 1990); metal adsorption to bacterial surfaces is predicted to account for over 90% of the overall Cd uptake.

To test the sensitivity of the *R. iodosum* adsorption model to variations in initial seawater compositions, several iterations were run for three different seawater conditions (Tables S2 and S4 [see footnote 1]). As expected, when initial seawater concentrations of trace metals are greater (i.e., for a simulated Paleoproterozoic seawater or seawater stoichiometrically fixed to *R. iodosum*), there is a greater amount of trace metals adsorbed to the surface of *R. iodosum*. Critically, however, for each of the three seawater conditions considered, assimilation remains at least an order of magnitude greater than adsorption for all elements considered here, except Cd as discussed already (data not shown). This suggests that the metal fluxes calculated here are reliant upon bacterial trace metal assimilation rather than surface adsorption and are thus relatively insensitive to minor shifts in the trace-metal composition of seawater or small changes in pH (see GSA Data Repository [see footnote 1]).

Trace-Element Assimilation by Other Phytoplankton and Potential Biomass Contributions to Banded Iron Formations

To put our work into context, we further compared the molar stoichiometry of metals assimilated by *R. iodosum*, as normalized to P,

$$P_{1000}Mn_{0.99}Co_{0.62}Ni_{0.74}Cu_{0.38}Zn_{6.41}Mo_{0.06}Cd_{0.0002},$$
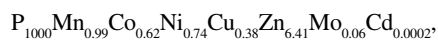
with the molar stoichiometry reported for natural marine cyanobacteria (lithogenic-corrected values from Walve et al., 2014, and data from references therein),

$$P_{1000}Mn_{1.26}Co_{0.02}Ni_{1.94}Cu_{0.42}Zn_{1.65}Mo_{0.49}Cd_{0.007},$$

as well as with the average stoichiometry for 15 marine eukaryotes (excluding the hard parts, using the volume-normalized average of Ho et al., 2003; where Ni is unavailable):

$$P_{1000}Mn_{3.5}Co_{0.20}Cu_{0.29}Zn_{0.67}Mo_{0.03}Cd_{0.14}.$$
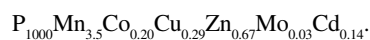
While we consider it extremely unlikely that eukaryotic phytoplankton contributed to banded iron formation deposition during the Paleoproterozoic, given that most estimates place eukaryote emergence well into the Proterozoic, we included them nonetheless to cover the range of photosynthetic biomass that might drive Fe(II) oxidation. For simplicity, we assumed a cellular volume of 100 µm^3 to calculate cell-specific trace-element loadings; in reality, the volumes can range from as low as 10 µm^3 for the green alga *Pycnococcus provasoli* to 7000 µm^3 for the diatom *Ditylum brightwellii* (Ho et al., 2003). Further, we acknowledge that phytoplankton C:P ratios and C:Zn ratios can vary widely, especially in cyanobacteria (e.g., Twining et al., 2004; Nuester et al., 2012; Reinhard et al., 2017). This variability will change the ratio of ferric iron to organic matter produced, but it will not change phytoplankton P to trace-metal ratios. Given that the evolution of phytoplankton C:P ratios is difficult to estimate (Planavsky, 2014; Reinhard et al., 2017), this adds some uncertainty to, but does not undermine, our approach.

Using the average cellular volume provided by Ho et al. (2003), and the same population of eukaryotic cells as cyanobacteria needed to produce the O$_2$ for annual banded iron formation deposition (4.5×10^{20} cells), we find an annual flux (in moles) of biomass-assimilated P (5.40×10^6), Zn (3.60×10^3), Co (1.08×10^3), Cu (1.58×10^3), Mo (1.40×10^2), Cd (7.65×10^2), and Mn (1.89×10^4) (see Table S5 [see footnote 1]). For cyanobacteria, using the same cell population, we calculate annual biomass contributions (mol yr^{-1}) via assimilation as follows: P (6.78×10^4), Zn (1.12×10^2), Co (1.47), Cu (2.86×10^1), Ni (1.31×10^2), Mo (3.32×10^1), Cd (4.86×10^{-1}), and Mn (8.55×10^1) (see Table 1E).

Considering the cell populations implicated for banded iron formation deposition by photoferrotrophic bacteria (1.9×10^{23} cells) or by cyanobacteria (4.5×10^{20} cells), we then used these cell-specific trace-element loadings to explore the trace-metal fluxes that biomass may have supplied to banded iron formations on an annual basis. Biomass-associated trace-element fluxes are presented in Figure 1A, alongside average trace-element fluxes implied for the Dales Gorge Member, as determined from a compilation of between 40 and 240 independent samples per trace element analyzed (cf. Table S1 [see footnote 1]). Assimilated trace metals associated with cyanobacteria and eukaryotes share some similarities, and for simplicity, trace metals that would have been associated with a eukaryotic population are not shown. It is immediately clear that for the minimum cell populations required for banded iron formation deposition, sinking biomass cannot account for
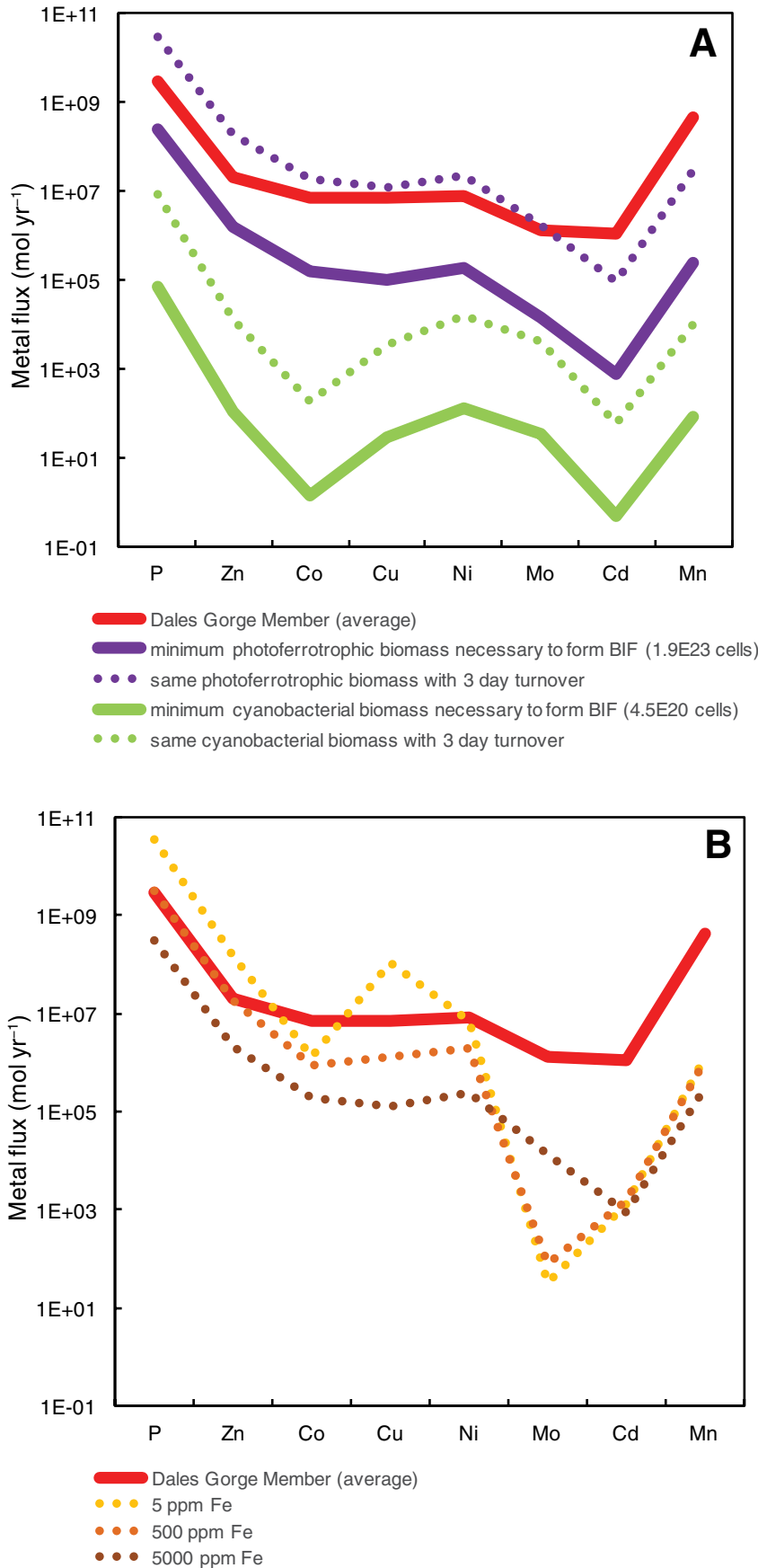
the entirety of the annual Dales Gorge Member exit flux of trace elements. In the case of *R. iodosum*, the calculated biomass falls short in P (by a factor of 12, i.e., 1/0.0830), Zn (14), Co (46), Cu (70), Ni (45), Mo (94), Cd (1510), and Mn (1831) (Table 1D).

However, it is important to note that these calculations assume that the minimum number of cells required to form the Dales Gorge Member experienced no turnover. In other words, the calculation of 1.91×10^{23} metabolizing cells of *R. iodosum* required to precipitate an annual banded iron formation layer assumes that each individual cell oxidized dissolved Fe(II) for an entire year, which would not be the case. Indeed, as in modern oceans, the population of marine phytoplankton in Paleoproterozoic surface waters was likely dynamic, with new growth occurring in lockstep with cell death to maintain a roughly stable population size. Doubling times of marine cyanobacteria are on the order of days, as fast as 3 d in culture under optimum conditions (Capone et al., 1997). Photoferrotrophs in culture show a similar range of doubling times (1–4 d; Wu et al., 2014). Assuming a 3 d doubling time, the entire population of cells would have been renewed ~121 times over the course of a year. This would have led to 2.31×10^{25} metabolizing cells yr^{-1}, and each would have its own trace-element–laden biomass. Under these conditions, the amount of trace elements that would have cycled annually through a dynamic population of photoferrotrophs maintaining the minimum cell population required for deposition of the Dales Gorge Member corresponds to the entirety of most trace elements preserved

Figure 1. (A) Comparison of the trace-element exit fluxes implicated in the deposition of the 2.48 Ga Dales Gorge Member banded iron formation (red line), with annual biomass-associated trace-element fluxes calculated for the photoferrotroph *Rhodovulum iodosum* for the minimal cell population (1.9×10^{23} cells; solid purple line) and one undergoing turnover every 3 d (2.31×10^{25} cells; stippled purple line), as well as for the average marine cyanobacterium with either minimal cell population (4.5×10^{20} cells; solid green line) or for one undergoing turnover every 3 d (5.45×10^{22} cells; stippled green line). (B) Exit fluxes and elemental fractionation calculated from surface complexation modeling of adsorption to varying concentrations of ferrihydrite from simulated seawater with photoferrotroph-like trace-element stoichiometry. BIF—banded iron formation. See text for details.

therein (Fig. 1A). By contrast, trace-element contributions from the marine cyanobacterial population required to form the banded iron formation fail to meet the observed banded iron formation exit fluxes, even with a 3 d doubling time (estimated at 5.45×10^{22} metabolizing cells), the highest observed in culture (Fig. 1A).

We also calculated trace-element fluxes that would have been associated with detrital contributions to the Dales Gorge Member (based on average Ti concentrations in the banded iron formation and assuming trace-element/Ti ratios corresponding to average continental crust; Table S6 [see footnote 1]), as well as hydrothermal fluxes to the Hamersley Basin photic zone (based on global hydrothermal inputs to seawater; Table S6 [see footnote 1]). With the exception of Mn, which, like Fe, has a strong hydrothermal source, neither detrital materials nor hydrothermal fluids appear to have been important in determining the trace-element composition of the banded iron formation for the elements considered in this study. Furthermore, irrespective of how trace elements may have been supplied to seawater, our calculations show that the entire banded iron formation inventory should have been cycled through biomass before being ultimately buried in the banded iron formation.

Trace-Element Contributions from Ferrihydrite to Banded Iron Formation

Several previous studies have considered the role played by the ferrihydrite particles undergoing sedimentation in the transfer of trace elements from the water column to the seafloor, where banded iron formation layers accumulated (e.g., Bjerrum and Canfield, 2002; Konhauser et al., 2009; Jones et al., 2015). To better understand this contribution, we used a surface protonation model for pure ferrihydrite and the metal binding constants of Dzombak and Morel (1990) to examine the extent of adsorption of the trace elements listed above for simulated seawater of various compositions; note, although the initial banded iron formation precipitate was likely a silica-rich ferrihydrite, or a ferric-silica gel (e.g., Zheng et al., 2016), there are no metal binding constants available for such a mineral phase. We then calculated the adsorptive loads associated with the amount of ferrihydrite estimated to have been deposited annually (7.85×10^{11} moles; Table 1F). In Figure 1B, we present the case for simulated seawater containing trace elements in photoferrotroph-like proportions to mimic a Paleoproterozoic water column where, like today, trace-elemental ratios in seawater reflected the average composition of phytoplankton (Sunda, 2012). We find that at low sorbent/sorbate ratios (low concentrations of ferrihydrite), adsorption is incomplete, and surface-adsorbed species are fractionated relative to the original fluid (Fig. 1B). As the sorbent/sorbate ratio increases, surface concentrations on ferrihydrite decrease (cf. the trend to lower elemental exit fluxes with increasing local ferrihydrite concentrations in Fig. 1B); however, elemental fractionation no longer occurs between ferrihydrite and the aqueous phase as adsorption trends toward 100% of available trace elements. In our adsorption models, this occurs between 500 and 5000 ppm Fe as ferrihydrite (Fig. 1B). Such high ferrihydrite concentrations represent systems far from equilibrium with respect to solubility limits on dissolved Fe(II).
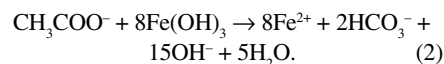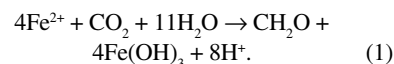
With ferric oxyhydroxide settling in the water column, these high sorbent/sorbate ratios are unlikely to have been met. However, quantitative sorption by ferrihydrite would take on a critical role in the uppermost portion of the sediment pile and during later diagenesis, when cell biomass was degraded, and biomass-associated trace elements were liberated to the sediment pore waters. In theory, oxide particle aggregation could also lead to local microenvironments with quantitative sorption, although this has not been demonstrated in modern ferruginous environments.

One issue that workers confront when using banded iron formation inventories as paleo-seawater proxies is whether the trace-element concentrations in banded iron formations are primary. Although it is possible to avoid analyzing banded iron formations that have undergone secondary enrichments by sampling rocks with preservation of sub-millimeter-scale primary sedimentary bedding and geochemical variations, while not selecting rocks with veining, recrystallized chert, martite formation, etc., it is more difficult to constrain the trace elements that may have left the system during early diagenesis and burial. In this regard, the effectiveness with which ferrihydrite at high concentrations can remove trace elements from pore water, and the fact that pore water retains a trace-element enrichment pattern resembling that of the source (in this case, seawater with trace elements in photoferrotroph-like proportions to simulate decaying biomass; Fig. 1B; Table 1) suggest that remobilization out of the sediments during burial is unlikely to have been significant in controlling trace-element signatures.

Recycling of Photoferrotrophic Biomass and Nutrient Supply

The idea that a standing population of phytoplankton may have undergone 100 or more population renewals through the course of the year has profound consequences for Fe recycling and the Fe:C ratio of the banded iron formation sediments. Both photoferrotrophy (Eq. 1) and DIR (Eq. 2) maintain a 4:1 Fe:C molar ratio, so for ferric iron to be preserved in banded iron formations as hematite and magnetite, the former must be deposited in a molar ratio with C that is in excess of 4:1 (Konhauser et al., 2005).

$$4Fe^{2+} + CO_2 + 11H_2O \rightarrow CH_2O + 4Fe(OH)_3 + 8H^+. \quad (1)$$

$$CH_3COO^- + 8Fe(OH)_3 \rightarrow 8Fe^{2+} + 2HCO_3^- + 15OH^- + 5H_2O. \quad (2)$$

This is achievable in two ways. First, some modern photoferrotrophic cells have been shown in experiments to remain in suspension after Fe(II) oxidation, with ferric iron particles preferentially settling out (Posth et al., 2010; Gauger et al., 2016). This implies that during times of banded iron formation deposition, such particles would have settled to the seafloor without the stoichiometric proportion of the cell biomass that produced them. Crucially, separated from its correspondent oxidant, and in the absence of sulfate in the Archean ocean (Crowe et al., 2014), this biomass would ultimately have been tied to another form of microbial respiration, such as methanogenesis (Konhauser et al., 2005), or it would have been buried in carbon-rich oxidant-poor sediments, such as black shales.

Second, much of the biomass (including cyanobacteria, other phototrophs, and nonphototrophs) was degraded prior to burial. Today, global organic carbon burial efficiencies are well below ~1% of net marine primary productivity (Raven and Falkowski, 1999), with most organic carbon respired using dissolved oxygen or sulfate as the terminal electron acceptors (Middelburg et al., 1993). With much lower dissolved oxygen and sulfate levels than modern values, it is thus likely that DIR was the predominant respiratory process during banded iron formation deposition (Johnson et al., 2008b). Based on the potential amount of biomass generated photoferrotrophically and the reducing equivalents required for magnetite formation, Konhauser et al. (2005) hypothesized that 3% of the phytoplankton biomass was buried and then oxidized within the sediment pile via DIR. More recent estimates using the C isotope and magnetite mass balance in banded iron formations have put C_{org} burial efficiencies at nearly 5% (Li et al., 2013).

An important consideration in our model is that if only 5% of the organic carbon produced by plankton in the photic zone was buried and then oxidized during late-stage diagenesis and

metamorphism, the other 95% was degraded while either settling through the shallow water column (~100 m for the continental shelf) or, most likely, once deposited as surface sediment at the seafloor. In anoxic waters and sediments below the photic zone, organic carbon degradation would likely have been dominated by fermentation, DIR, and methanogenesis. The importance of these metabolisms cannot be overstated, because they can result in the rapid decomposition of phytoplankton biomass to produce fermentation products (e.g., H_2, lactate, acetate, CO_2), dissolved bicarbonate, or methane gas, and the trace elements originally associated with the biomass would have then been released back into the water column or sediment pore waters, while the ferric oxyhydroxides accumulated as banded iron formation sediment. Indeed, in modern anoxic tidal flats, ^{13}C-labeled glucose has been shown to be almost completely fermented within just 2 d to acetate, ethanol, formate, and H_2 (Graue et al., 2012). Moreover, in Kabuno Bay, Democratic Republic of the Congo, fermentation, sulfate reduction, and methanogenesis occur alongside DIR, and the net result is that ferric oxyhydroxides escape reduction and make it out of the photic zone (Llirós et al., 2015).

In short, we argue that decaying biomass was likely an important source of trace elements to the Dales Gorge Member, and that standing stocks of phytoplankton, especially photoferrotrophic biomass, would have been capable of supplying this flux. Remineralization of their biomass would have liberated trace elements back into the water column to feed further picoplankton growth (and these elements are thus not recorded in banded iron formation sediments unless adsorbed to settling ferric oxyhydroxides), or if they were liberated to sediment pore waters, the biomass-associated trace elements would have been fixed into banded iron formation sediments by sorption to iron oxyhydroxides.

Interestingly, many trace elements in modern marine environments exhibit nutrient-like behavior (e.g., Cd, Cu, Ni, Zn), meaning that they are generally drawn down to nanomolar concentrations in the photic zone because of biological utilization. With increasing depth in the water column, they are then liberated from sinking biomass via organic matter remineralization (Suess, 1980; Henrichs and Reeburgh, 1987), thus leading to their regeneration and enrichment in deeper waters at elemental ratios reflecting the average composition of phytoplankton (e.g., Bruland and Lohan, 2003; Sunda, 2012; Biller and Bruland, 2013). Accordingly, there is a strong correlation between intracellular and dissolved seawater elemental stoichiometries in modern marine environments (Moore et al., 2013). As these deeper waters are again brought onto the shelf, the trace elements fuel further picoplanktonic growth. However, where banded iron formation depositional settings differed is that they formed in relatively shallow waters, where perhaps the majority of recycling could have taken place at the seafloor, and where the accumulated mass of precursor phases to banded iron formation sediment (ferric oxyhydroxides) then acquired the biologically controlled trace-element stoichiometries in bottom water or pore waters. Through these processes, we propose that banded iron formation sediments themselves may have become a permanent recorder of ancient phytoplanktonic trace-element requirements and activity.

CONCLUSIONS

The strong biological requirement for trace elements by marine phytoplankton promotes the export of these elements from the photic zone. Using new constraints on trace-element assimilation and adsorption by photoferrotrophs, we demonstrate that photoferrotroph populations in the past would have cycled annual amounts of trace elements that are comparable to the total banded iron formation exit flux. Remineralization through a combination of fermentation, DIR, and methanogenesis then would have liberated significant quantities of trace elements back into the pore waters, where near-quantitative sorption by the vast amounts of deposited ferrihydrite would have locked those trace elements into the banded iron formation record. While adsorption to iron minerals remains an important mechanism for the ultimate capture of trace elements in banded iron formation precursor sediments, the same photoferrotroph populations implicated in banded iron formation deposition should have cycled the entirety of these trace elements through their biomass prior to banded iron formation deposition, suggesting a new role for banded iron formation archives as a potential recorder of ancient phytoplanktonic activity.

REFERENCES CITED

Ahn, J.H., and Buseck, P.R., 1990, Hematite nanospheres of possible colloidal origin from a Precambrian banded iron formation: Science, v. 250, p. 111–113, https://doi.org/10.1126/science.250.4977.111.

Alibert, C., and McCulloch, 1993, Rare earth element and neodymium isotopic compositions of the banded iron-formations and associated shales from Hamersley, Western Australia: Geochimica et Cosmochimica Acta, v. 57, p. 187–204, https://doi.org/10.1016/0016-7037(93)90478-F.

Bekker, A., Slack, J.F., Planavsky, N., Krapež, B., Hofmann, A., Konhauser, K.O., and Rouxel, O.J., 2010, Iron formation: A sedimentary product of the complex interplay among mantle, tectonic, and biospheric processes: Economic Geology and the Bulletin of the Society of Economic Geologists, v. 105, p. 467–508, https://doi.org/10.2113/gsecongeo.105.3.467.

Bekker, A., Planavsky, N.J., Krapež, B., Rasmussen, B., Hofmann, A., Slack, J.F., Rouxel, O.J., and Konhauser, K.O., 2014, Iron formations: Their origins and implications for ancient seawater chemistry, in Holland, H.D., and Turekian, K.K., eds., Treatise in Geochemistry (2nd ed.): Amsterdam, Elsevier, p. 561–628, https://doi.org/10.1016/B978-0-08-095975-7.00719-1.

Biebl, H., and Pfennig, N., 1978, Growth yields of green sulfur bacteria in mixed cultures with sulfur and sulfate reducing bacteria: Journal of Microbiology (Seoul, Korea), v. 117, p. 9–16.

Biller, D.V., and Bruland, K.W., 2013, Sources and distributions of Mn, Fe, Co, Ni, Cu, Zn, and Cd relative to macronutrients along the central California coast during the spring and summer upwelling season: Marine Chemistry, v. 155, p. 50–70, https://doi.org/10.1016/j.marchem.2013.06.003.

Bjerrum, C.J., and Canfield, D.E., 2002, Ocean productivity before about 1.9 Gyr ago limited by phosphorus adsorption onto iron oxides: Nature, v. 417, p. 159–162, https://doi.org/10.1038/417159a.

Blättler, C.L., Kump, L.R., Fischer, W.W., Paris, G., Kasbohm, J.J., and Higgins, J.A., 2017, Constraints on ocean carbonate chemistry and pCO$_2$ in the Archaean and Palaeoproterozoic: Nature Geoscience, v. 10, p. 41–45, https://doi.org/10.1038/ngeo2844.

Borrok, D.M., Fein, J.B., and Kulpa, C.F., 2004a, Cd and proton adsorption onto bacterial consortia grown from industrial wastes and contaminated geologic settings: Environmental Science & Technology, v. 38, p. 5656–5664, https://doi.org/10.1021/es049679n.

Borrok, D.M., Fein, J.B., and Kulpa, C.F., 2004b, Proton and Cd adsorption onto natural bacterial consortia: Testing universal adsorption behavior: Geochimica et Cosmochimica Acta, v. 68, p. 3231–3238, https://doi.org/10.1016/j.gca.2004.02.003.

Bruland, K.W., 1992, Complexation of cadmium by natural organic ligands in the central North Pacific: Limnology and Oceanography, v. 37, p. 1008–1017, https://doi.org/10.4319/lo.1992.37.5.1008.

Bruland, K.W., and Lohan, M.C., 2003, Controls of trace metals in seawater, in Holland, H.D., and Turekian, K., eds., Treatise on Geochemistry, Volume 6: Amsterdam, Elsevier, p. 23–47, https://doi.org/10.1016/b0-08-043751-6/06105-3.

Bruland, K.W., Donat, J.R., and Hutchins, D.A., 1991, Interactive influences of bioactive trace metals on biological production in oceanic waters: Limnology and Oceanography, v. 36, p. 1555–1577, https://doi.org/10.4319/lo.1991.36.8.1555.

Byrne, R.H., Kump, L.R., and Cantrell, K.J., 1988, The influence of temperature and pH on trace metal speciation in seawater: Marine Chemistry, v. 25, p. 163–181, https://doi.org/10.1016/0304-4203(88)90062-X.

Capone, D.G., Zehr, J.P., Paerl, H.W., Bergman, B., and Carpenter, E.J., 1997, *Trichodesmium*, a globally significant marine cyanobacterium: Science, v. 276, p. 1221–1229, https://doi.org/10.1126/science.276.5316.1221.

Chan, C.S., Emerson, D., and Luther, G.W., 2016, The role of microaerophilic Fe-oxidizing micro-organisms in producing banded iron formations: Geobiology, v. 14, p. 509–528, https://doi.org/10.1111/gbi.12192.

Cloud, P., 1973, Paleoecological significance of the banded iron-formation: Economic Geology and the Bulletin of the Society of Economic Geologists, v. 68, p. 1135–1143, https://doi.org/10.2113/gsecongeo.68.7.1135.

Crowe, S.A., Jones, C., Katsev, S., Magen, C., O'Neill, A., Sturm, A., Canfield, D., Haffner, G., Mucci, A., and Sundby, B., 2008, Photoferrotrophs thrive in an Archean ocean analogue: Proceedings of the National Academy of Sciences of the United States of America, v. 105, p. 15,938–15,943, https://doi.org/10.1073/pnas.0805313105.

Crowe, S.A., Katsev, S., Leslie, K., Sturm, A., Magen, C., Nomosatryo, S., Pack, M.A., Kessler, J.D., Reeburgh, W.S., Roberts, J.A., González, L., Haffner, G.D., Mucci, A., Sundby, B., et al., 2011, The methane cycle in ferruginous Lake Matano: Geobiology, v. 9, p. 61–78, https://doi.org/10.1111/j.1472-4669.2010.00257.x.

Crowe, S.A., Døssing, L.N., Beukes, N.J., Bau, M., Kruger, S.J., Frei, R., and Canfield, D.E., 2013, Atmospheric oxygenation three billion years ago: Nature, v. 501, p. 535–538, https://doi.org/10.1038/nature12426.

Crowe, S.A., Paris, G., Katsev, S., Jones, C., Kim, S.-T., Zerkle, A.L., Nomosatryo, S., Fowle, D.A., Adkins, J.F., Sessions, A.L., Farquhar, J., and Canfield, D.E., 2014, Sulfate was a trace constituent of Archean seawater: Science, v. 346, p. 735–739, https://doi.org/10.1126/science.1258966.

Dittrich, M., and Sibler, S., 2005, Cell surface groups of two picocyanobacteria strains studied by zeta potential investigations, potentiometric titration, and infrared spectroscopy: Journal of Colloid and Interface Science, v. 286, p. 487–495, https://doi.org/10.1016/j.jcis.2005.01.029.

Dzombak, D.A., and Morel, F.M.M., 1990, Surface Complexation Modeling: New York, Wiley-Interscience, 393 p.

Ehrenreich, A., and Widdel, F., 1994, Anaerobic oxidation of ferrous iron by purple bacteria, a new type of phototrophic metabolism: Applied and Environmental Microbiology, v. 60, p. 4517–4526.

Eickhoff, M., Obst, M., Schröder, C., Hitchcock, A.P., Tyliszczak, T., Martinez, R.E., Robbins, L.J., Konhauser, K.O., and Kappler, A., 2014, Nickel partitioning in biogenic and abiogenic ferrihydrite: The influence of silica and implications for ancient environments: Geochimica et Cosmochimica Acta, v. 140, p. 65–79, https://doi.org/10.1016/j.gca.2014.05.021.

Ewers, W.E., and Morris, R.C., 1981, Studies of the Dales Gorge Member of the Brockman Iron Formation, Western Australia: Economic Geology and the Bulletin of the Society of Economic Geologists, v. 76, p. 1929–1953, https://doi.org/10.2113/gsecongeo.76.7.1929.

Fein, J., Martin, A., and Wightman, P., 2001, Metal adsorption onto bacterial surfaces: Development of a predictive approach: Geochimica et Cosmochimica Acta, v. 65, p. 4267–4273, https://doi.org/10.1016/S0016-7037(01)00721-9.

Frei, R., Crowe, S.A., Bau, M., Polat, A., Fowle, D.A., and Døssing, L.N., 2016, Oxidative elemental cycling under the low O$_2$ Eoarchean atmosphere: Scientific Reports, v. 6, https://doi.org/10.1038/srep21058.

Fru, E.C., Rodríguez, N.P., Partin, C.A., Lalonde, S., Andersson, P., Weiss, D.J., Abderrazak, E.A., Rodushkin, I., and Konhauser, K.O., 2016, Cu isotopes in marine black shales record the Great Oxidation Event: Proceedings of the National Academy of Sciences of the United States of America, v. 113, p. 4941–4946, https://doi.org/10.1073/pnas.1523544113.

Garrels, R.M., and Perry, E.A.J., 1974, Cycling of carbon, sulfur, and oxygen through geologic time, *in* Goldberg, E.A., ed., The Sea: New York, Wiley, p. 303–336.

Gauger, T., Byrne, J.M., Konhauser, K.O., Obst, M., Crowe, S.A., and Kappler, A., 2016, Influence of organics and silica on Fe(II) oxidation rates and cell-mineral aggregate formation by the green-sulfur Fe(II)-oxidizing bacterium *Chlorobium ferrooxidans* KoFox—Implications for Fe(II) oxidation in ancient oceans: Earth and Planetary Science Letters, v. 443, p. 81–89, https://doi.org/10.1016/j.epsl.2016.03.022.

Graue, J., Engelen, B., and Cypionka, H., 2012, Degradation of cyanobacterial biomass in anoxic tidal-flat sediments: A microcosm study of metabolic processes and community changes: Multidisciplinary Journal of Microbial Ecology, v. 6, p. 660–669.

Grotzinger, J.P., and Kasting, J.F., 1993, New constraints on Precambrian ocean composition: The Journal of Geology, v. 101, p. 235–243, https://doi.org/10.1086/648218.

Gustafsson, J.P., 2013, Visual Minteq: http://www.lwr.kth.se/English/OurSoftware/vminteq/ (accessed April 2017).

Hadjoudja, S., Deluchat, V., and Baudu, M., 2010, Cell surface characterisation of *Microcystis aeruginosa* and *Chlorella vulgaris*: Journal of Colloid and Interface Science, v. 342, p. 293–299, https://doi.org/10.1016/j.jcis.2009.10.078.

Hallbeck, L., and Pedersen, K., 1991, Autotrophic and mixotrophic growth of *Gallionella ferruginea*: Microbiology, v. 137, p. 2657–2661, https://doi.org/10.1099/00221287-137-11-2657.

Han, T.M., 1988, Origin of magnetite in Precambrian iron-formations of low metamorphic grade, *in* Zachrisson, E., ed., Proceedings of the Seventh Quadrennial IAGOD Symposium: Stuttgart, Germany, E. Schweizerbart'che Verlagsbachhandlung, p. 641–656.

Hao, L., Li, J., Kappler, A., and Obst, M., 2013, Mapping of heavy metal ion sorption to cell-extracellular polymeric substance–mineral aggregates by using metal-selective fluorescent probes and confocal laser scanning microscopy: Applied and Environmental Microbiology, v. 79, p. 6524–6534, https://doi.org/10.1128/AEM.02454-13.

Hegler, F., Posth, N.R., Jiang, J., and Kappler, A., 2008, Physiology of phototrophic iron(II)-oxidizing bacteria: Implications for modern and ancient environments: FEMS Microbiology Ecology, v. 66, p. 250–260, https://doi.org/10.1111/j.1574-6941.2008.00592.x.

Heimann, A., Johnson, C.M., Beard, B.L., Valley, J.W., Roden, E.E., Spicuzza, M.J., and Beukes, N.J., 2010, Fe, C, and O isotope compositions of banded iron formation carbonates demonstrate a major role for dissimilatory iron reduction in ~ 2.5 Ga marine environments: Earth and Planetary Science Letters, v. 294, p. 8–18, https://doi.org/10.1016/j.epsl.2010.02.015.

Henrichs, S.M., and Reeburgh, W.S., 1987, Anaerobic mineralization of marine sediment organic matter: Rates and the role of anaerobic processes in the oceanic carbon economy: Geomicrobiology Journal, v. 5, p. 191–237, https://doi.org/10.1080/01490458709385971.

Ho, T.Y., Quigg, A., Finkel, Z.V., Milligan, A.J., Wyman, K., Falkowski, P.G., and Morel, F.M.M., 2003, The elemental composition of some marine phytoplankton: Journal of Phycology, v. 39, p. 1145–1159, https://doi.org/10.1111/j.0022-3646.2003.03-090.x.

Huberty, J.M., Konishi, H., Heck, P.R., Fournelle, J.H., Valley, J.W., and Xu, H., 2012, Silician magnetite from the Dales Gorge Member of the Brockman Iron Formation, Hamersley Group, Western Australia: The American Mineralogist, v. 97, p. 26–37, https://doi.org/10.2138/am.2012.3864.

Jacquet, S., Lennon, J.-F., Marie, D., and Vaulot, D., 1998, Picoplankton population dynamics in coastal waters of the northwestern Mediterranean Sea: Limnology and Oceanography, v. 43, p. 1916–1931, https://doi.org/10.4319/lo.1998.43.8.1916.

James, H.L., 1954, Sedimentary facies of iron-formation: Economic Geology and the Bulletin of the Society of Economic Geologists, v. 49, p. 235–293, https://doi.org/10.2113/gsecongeo.49.3.235.

Johnson, C.M., Beard, B.L., Klein, C., Beukes, N.J., and Roden, E.E., 2008a, Iron isotopes constrain biologic and abiologic processes in banded iron formation genesis: Geochimica et Cosmochimica Acta, v. 72, p. 151–169, https://doi.org/10.1016/j.gca.2007.10.013.

Johnson, C.M., Beard, B.L., and Roden, E.E., 2008b, The iron isotope fingerprints of redox and biogeochemical cycling in the modern and ancient Earth: Annual Review of Earth and Planetary Sciences, v. 36, p. 457–493, https://doi.org/10.1146/annurev.earth.36.031207.124139.

Jones, C., Nomosatryo, S., Crowe, S.A., Bjerrum, C.J., and Canfield, D.E., 2015, Iron oxides, divalent cations, silica, and the early Earth phosphorus crisis: Geology, v. 43, p. 135–138, https://doi.org/10.1130/G36044.1.

Kappler, A., Pasquero, C., Konhauser, K.O., and Newman, D.K., 2005, Deposition of banded iron formations by anoxygenic phototrophic Fe(II)-oxidizing bacteria: Geology, v. 33, p. 865–868, https://doi.org/10.1130/G21658.1.

Köhler, I., Konhauser, K.O., and Kappler, A., 2010, Role of microorganisms in banded iron formations, *in* Barton, L., Mandl, M., and Loy, A., eds., Geomicrobiology: Molecular and Environmental Perspective: Dordrecht, Springer Science + Business Media, p. 309–324, https://doi.org/10.1007/978-90-481-9204-5_14.

Köhler, I., Konhauser, K.O., Papineau, D., Bekker, A., and Kappler, A., 2013, Biological carbon precursor to diagenetic siderite with spherical structures in iron formations: Nature Communications, v. 4, p. 1741–1747, https://doi.org/10.1038/ncomms2770.

Konhauser, K.O., Hamade, T., Raiswell, R., Morris, R., Ferris, F., Southam, G., and Canfield, D., 2002, Could bacteria have formed the Precambrian banded iron formations?: Geology, v. 30, p. 1079–1082, https://doi.org/10.1130/0091-7613(2002)030<1079:CBHFTP>2.0.CO;2.

Konhauser, K.O., Newman, D., and Kappler, A., 2005, The potential significance of microbial Fe(III) reduction during deposition of Precambrian banded iron formations: Geobiology, v. 3, p. 167–177, https://doi.org/10.1111/j.1472-4669.2005.00055.x.

Konhauser, K.O., Lalonde, S.V., Amskold, L.A., and Holland, H., 2007a, Was there really an Archean phosphate crisis?: Science, v. 315, p. 1234.

Konhauser, K.O., Amskold, L.A., Lalonde, S.V., Posth, N., Kappler, A., and Anbar, A.D., 2007b, Decoupling photochemical Fe(II) oxidation from shallow-water BIF deposition: Earth and Planetary Science Letters, v. 258, p. 87–100, https://doi.org/10.1016/j.epsl.2007.03.026.

Konhauser, K.O., Pecoits, E., Lalonde, S.V., Papineau, D., Nisbet, E.G., Barley, M.E., Arndt, N.T., Zahnle, K., and Kamber, B.S., 2009, Oceanic nickel depletion and a methanogen famine before the Great Oxidation Event: Nature Geoscience, v. 458, p. 750–753, https://doi.org/10.1038/nature07858.

Konhauser, K.O., Lalonde, S.V., Planavsky, N.J., Pecoits, E., Lyons, T.W., Mojzsis, S.J., Rouxel, O.J., Barley, M.E., Rosière, C.A., Fralick, P.W., Kump, L.R., and Bekker, A., 2011, Aerobic bacterial pyrite oxidation and acid rock drainage during the Great Oxidation Event: Nature Geoscience, v. 478, p. 369–373, https://doi.org/10.1038/nature10511.

Konhauser, K.O., Robbins, L.J., Pecoits, E., Peacock, C., Kappler, A., and Lalonde, S.V., 2015, The Archean nickel famine revisited: Astrobiology, v. 15, p. 804–815, https://doi.org/10.1089/ast.2015.1301.

Konhauser, K.O., Planavsky, N.J., Hardisty, D., Robbins, L.J., Warchola, T.J., Haugaard, R., Lalonde, S.V., Partin, C.A., Oonk, P.B.H., Tsikos, H., Lyons, T.W., Bekker, A., and Johnson, C.M., 2017, Iron formations: A record of Neoarchean to Paleoproterozoic environmental history: Earth-Science Reviews, v. 172, p. 140–177, https://doi.org/10.1016/j.earscirev.2017.06.012.

Krapež, B., Barley, M.E., and Pickard, A.L., 2003, Hydrothermal and resedimented origins of the precursor sediments to banded iron formations: Sedimentological evidence from the early Palaeoproterozoic Brockman supersequence of Western Australia: Sedimentology, v. 50, p. 979–1011, https://doi.org/10.1046/j.1365-3091.2003.00594.x.

Kuntz, L.B., Laakso, T.A., Schrag, D.P., and Crowe, S.A., 2015, Modeling the carbon cycle in Lake Matano: Geobiology, v. 13, p. 454–461, https://doi.org/10.1111/gbi.12141.

Li, W., Huberty, J., Beard, B., Valley, J., and Johnson, C., 2013, Contrasting behavior of oxygen and iron isotopes in banded iron formations as determined by in situ isotopic analysis: Earth and Planetary Science Letters, v. 384, p. 132–143, https://doi.org/10.1016/j.epsl.2013.10.014.

Li, Y.L., Konhauser, K.O., Cole, D.R., and Phelps, T.J., 2011, Mineral ecophysiological data provide growing evidence for microbial activity in banded-iron formations: Geology, v. 39, p. 707–710, https://doi.org/10.1130/G32003.1.

Liu, Y., Alessi, D.S., Owttrim, G.W., and Petrash, D.A., 2015, Cell surface reactivity of *Synechococcus* sp. PCC 7002: Implications for metal sorption from seawater: Geochimica et Cosmochimica Acta, v. 169, p. 30–44, https://doi.org/10.1016/j.gca.2015.07.033.

Llirós, M., Armisen, T.G., Darchambeau, F., Morana, C., Margarit, X.T., Inceoğlu, Ö., Borrego, C.M., Bouillon, S., Servais, P., Borges, A.V., Descy, J.P., Canfield, D.E., and Crowe, S.A., 2015, Pelagic photoferrotrophy and iron cycling in a modern ferruginous basin: Scientific Reports, v. 5, p. 13803, https://doi.org/10.1038/srep13803.

Martell, A.E., and Smith, R.M., 1977, Critical Stability Constants: Volume 3. Other Organic Ligands: New York, Plenum, 496 p.

Martinez, R.E., Konhauser, K.O., Paunova, N., Wu, W., Alessi, D.S., and Kappler, A., 2016, Surface reactivity of the anaerobic phototrophic Fe(II)-oxidizing bacterium *Rhodovulum iodosum*: Implications for trace metal budgets in ancient oceans and banded iron formations: Chemical Geology, v. 442, p. 113–120, https://doi.org/10.1016/j.chemgeo.2016.09.004.

Middelburg, J.J., Vlug, T., Jaco, F., and van der Nat, W.A., 1993, Organic matter mineralization in marine systems: Global and Planetary Change, v. 8, p. 47–58, https://doi.org/10.1016/0921-8181(93)90062-S.

Mikutta, R., Baumgärtner, A., Schippers, A., Haumaier, L., and Guggenberger, G., 2012, Extracellular polymeric substances from *Bacillus subtilis* associated with minerals modify the extent and rate of heavy metal sorption: Environmental Science & Technology, v. 46, p. 3866–3873, https://doi.org/10.1021/es204471x.

Miyazono, A., Odate, T., and Maita, Y., 1992, Seasonal fluctuations of cell density of cyanobacteria and other picophytoplankton in Iwanai Bay, Hokkaido, Japan: Journal of Oceanography, v. 48, p. 257–266, https://doi.org/10.1007/BF02233986.

Moon, E.M., and Peacock, C.L., 2013, Modelling Cu(II) adsorption to ferrihydrite and ferrihydrite–bacteria composites: Deviation from additive adsorption in the composite sorption system: Geochimica et Cosmochimica Acta, v. 104, p. 148–164, https://doi.org/10.1016/j.gca.2012.11.030.

Moore, C.M., Mills, M.M., Arrigo, K.R., Berman-Frank, I., Bopp, L., Boyd, P.W., Galbraith, E.D., Geider, R.J., Guieu, C., Jaccard, S.L., Jickells, T.D., La Roche, J., Lenton, T.M., Mahowald, N.M., et al., 2013, Processes and patterns of oceanic nutrient limitation: Nature Geoscience, v. 6, no. 9, p. 701–710, https://doi.org/10.1038/ngeo1765.

Nuester, J., Vogt, S., Newville, M., Kustka, A.B., and Twining, B.S., 2012, The unique biogeochemical signature of the marine diazotroph *Trichodesmium*: Frontiers in Microbiology, v. 3, 150, 15 p., https://doi.org/10.3389/fmicb.2012.00150.

Olson, S.L., Kump, L.R., and Kasting, J.F., 2013, Quantifying the areal extent and dissolved oxygen concentrations of Archean oxygen oases: Chemical Geology, v. 362, p. 35–43, https://doi.org/10.1016/j.chemgeo.2013.08.012.

Pai, S.C., and Chen, H.Y., 1994, Vertical distribution of cadmium in marginal seas of the western Pacific Ocean: Marine Chemistry, v. 47, p. 81–91, https://doi.org/10.1016/0304-4203(94)90015-9.

Pecoits, E., Gingras, M.K., Barley, M.E., Kappler, A., Posth, N., and Konhauser, K.O., 2009, Petrography and geochemistry of the Dales Gorge banded iron formation: Paragenetic sequence, source and implications for palaeo-ocean chemistry: Precambrian Research, v. 172, p. 163–187, https://doi.org/10.1016/j.precamres.2009.03.014.

Pecoits, E., Smith, M.L., Catling, D.C., Philippot, P., Kappler, A., and Konhauser, K.O., 2015, Atmospheric hydrogen peroxide and Eoarchean iron formations: Geobiology, v. 13, p. 1–14, https://doi.org/10.1111/gbi.12116.

Percak-Dennett, L., Roden, E.E., Beard, B.L., and Johnson, C.M., 2011, Iron isotope fractionation during dissimilatory iron reduction under simulated Archean conditions: Geobiology, v. 9, p. 205–220, https://doi.org/10.1111/j.1472-4669.2011.00277.x.

Planavsky, N.J., 2014, The elements of marine life: Nature Geoscience, v. 7, p. 855–856, https://doi.org/10.1038/ngeo2307.

Planavsky, N., Rouxel, O.J., Bekker, A., Hofmann, A., Little, C.T.S., and Lyons, T.W., 2012, Iron isotope composition of some Archean and Proterozoic iron formations: Geochimica et Cosmochimica Acta, v. 80, p. 158–169, https://doi.org/10.1016/j.gca.2011.12.001.

Planavsky, N.J., Asael, D., Hofmann, A., Reinhard, C.T., Lalonde, S.V., Knudsen, A., Wang, X., Ossa Ossa, F., Pecoits, E., Smith, A.J.B., Beukes, N.J., Bekker, A., Johnson, T.M., Konhauser, K.O., et al., 2014, Evidence for oxygenic photosynthesis half a billion years before the Great Oxidation Event: Nature Geoscience, v. 7, p. 283–286, https://doi.org/10.1038/ngeo2122.

Posth, N.R., Huelin, S., Konhauser, K.O., and Kappler, A., 2010, Size, density and composition of cell–mineral aggregates formed during anoxygenic phototrophic Fe(II) oxidation: Impact on modern and ancient environments: Geochimica et Cosmochimica Acta, v. 74, p. 3476–3493, https://doi.org/10.1016/j.gca.2010.02.036.

Posth, N.R., Konhauser, K.O., and Kappler, A., 2013, Microbiological processes in banded iron formation deposition: Sedimentology, v. 60, p. 1733–1754, https://doi.org/10.1111/sed.12051.

Price, N.M., and Morel, F.M.M., 1990, Cadmium and cobalt substitution for zinc in a marine diatom: Nature Geoscience, v. 344, p. 658–660.

Rasmussen, B., Krapež, B., Muhling, J.R., and Suvorova, A., 2015, Precipitation of iron silicate nanoparticles in early Precambrian oceans marks Earth's first iron age: Geology, v. 43, p. 303–306, https://doi.org/10.1130/G36309.1.

Rasmussen, B., Muhling, J.R., Suvorova, A., and Krapež, B., 2016, Dust to dust: Evidence for the formation of "primary" hematite dust in banded iron formations via oxidation of iron silicate nanoparticles: Precambrian Research, v. 284, p. 49–63, https://doi.org/10.1016/j.precamres.2016.07.003.

Rasmussen, B., Muhling, J.R., Suvorova, A., and Krapež, B., 2017, Greenalite precipitation linked to the deposition of banded iron formations downslope from a late Archean carbonate platform: Precambrian Research, v. 290, p. 49–62, https://doi.org/10.1016/j.precamres.2016.12.005.

Raven, J.A., and Falkowski, P.G., 1999, Oceanic sinks for atmospheric CO_2: Plant, Cell & Environment, v. 22, p. 741–755, https://doi.org/10.1046/j.1365-3040.1999.00419.xx.

Reddy, T.R., Zheng, X.-Y., Roden, E.E., Beard, B.L., and Johnson, C.M., 2016, Silicon isotope fractionation during microbial reduction of Fe(III)-Si gels under Archean seawater conditions and implications for iron formation genesis: Geochimica et Cosmochimica Acta, v. 190, p. 85–99, https://doi.org/10.1016/j.gca.2016.06.035.

Reinhard, C.T., Planavsky, N.J., Gill, B.C., Ozaki, K., Robbins, L.J., Lyons, T.W., Fischer, W.W., Wang, C., Cole, D.B., and Konhauser, K.O., 2017, Evolution of the global phosphorous cycle: Nature, v. 541, p. 386–389, https://doi.org/10.1038/nature20772.

Robbins, L.J., Lalonde, S.V., Saito, M.A., Planavsky, N.J., Mloszewska, A.M., Pecoits, E., Scott, C., Dupont, C.L., Kappler, A., and Konhauser, K.O., 2013, Authigenic iron oxide proxies for marine zinc over geological time and implications for eukaryotic metallome evolution: Geobiology, v. 11, p. 295–306, https://doi.org/10.1111/gbi.12036.

Saito, M.A., Sigman, D.M., and Morel, F.M.M., 2003, The bioinorganic chemistry of the ancient ocean: The co-evolution of cyanobacterial metal requirements and biogeochemical cycles at the Archean-Proterozoic boundary?: Inorganica Chimica Acta, v. 356, p. 308–318, https://doi.org/10.1016/S0020-1693(03)00442-0.

Sañudo-Wilhelmy, S.A., Tovar-Sanchez, A., and Fu, F.X., 2004, The impact of surface-adsorbed phosphorus on phytoplankton Redfield stoichiometry: Nature, v. 432, p. 897–901, https://doi.org/10.1038/nature03125.

Satkoski, A.M., Beukes, N.J., Li, W., Beard, B.L., and Johnson, C.M., 2015, A redox-stratified ocean 3.2 billion years ago: Earth and Planetary Science Letters, v. 430, p. 43–53, https://doi.org/10.1016/j.epsl.2015.08.007.

Scott, C.T., Planavsky, N.J., Dupont, C.L., Kendall, B., Gill, B.C., Robbins, L.J., Husband, K.F., Arnold, G.L., Wing, B.A., Poulton, S.W., Bekker, A., Anbar, A.D., Konhauser, K.O., and Lyons, T.W., 2013, Bioavailability of zinc in marine systems through time: Nature Geoscience, v. 6, p. 125–128, https://doi.org/10.1038/ngeo1679.

Straub, K., Rainey, F., and Widdel, F., 1999, *Rhodovulum iodosum* sp. nov. and *Rhodovulum robiginosum* sp.

nov., two new marine phototrophic ferrous-iron–oxidizing purple bacteria: International Journal of Systematic Bacteriology, v. 49, p. 729–735, https://doi.org/10.1099/00207713-49-2-729.

Suess, E., 1980, Particulate organic carbon flux in the oceans—Surface: Nature, v. 288, p. 260–263, https://doi.org/10.1038/288260a0.

Sun, S., Konhauser, K.O., Kappler, A., and Yiliang, L., 2015, Primary hematite in Neoarchean to Paleoproterozoic oceans: Geological Society of America Bulletin, v. 127, p. 850–861, https://doi.org/10.1130/B31122.1.

Sunda, W.G., 2012, Feedback interactions between trace metal nutrients and phytoplankton in the ocean: Frontiers in Microbiology, v. 3, 204, 22 p., https://doi.org/10.3389/fmicb.2012.00204.

Swanner, E.D., Planavsky, N., Lalonde, S.V., Robbins, L.J., Bekker, A., Rouxel, O., Saito, M.A., Kappler, A., Mojzsis, S.J., and Konhauser, K.O., 2014, Cobalt and marine redox evolution: Earth and Planetary Science Letters, v. 390, p. 253–263, https://doi.org/10.1016/j.epsl.2014.01.001.

Swanner, E.D., Mloszewska, A.M., Cirpka, O.A., Schoenberg, R., Konhauser, K.O., and Kappler, A., 2015, Modulation of oxygen production in Archaean oceans by episodes of Fe(II) toxicity: Nature Geoscience, v. 8, p. 126–130, https://doi.org/10.1038/ngeo2327.

Tang, T., Fadaei, H., and Hu, Z., 2014, Rapid evaluation of algal and cyanobacterial activities through specific oxygen production rate measurement: Ecological Engineering, v. 73, p. 439–445, https://doi.org/10.1016/j.ecoleng.2014.09.095.

Tosca, N.J., Guggenheim, S., and Pufahl, P.K., 2016, An authigenic origin for Precambrian greenalite: Implications for iron formation and the chemistry of ancient seawater: Geological Society of America Bulletin, v. 128, p. 511–530, https://doi.org/10.1130/B31339.1.

Trendall, A.F., and Blockley, J.G., 1970, The Iron Formations of the Precambrian Hamersley Group Western Australia with Special Reference to the Associated Crocidolite: Geological Survey of Western Australia Bulletin 119, 366 p.

Twining, B.S., Baines, S.B., and Fisher, N.S., 2004, Element stoichiometries of individual plankton cells collected during the Southern Ocean Iron Experiment (SOFeX): Limnology and Oceanography, v. 49, p. 2115–2128, https://doi.org/10.4319/lo.2004.49.6.2115.

Walve, J., Gelting, J., and Ingri, J., 2014, Trace metals and nutrients in Baltic Sea cyanobacteria: Internal and external fractions and potential use in nitrogen fixation: Marine Chemistry, v. 158, p. 27–38, https://doi.org/10.1016/j.marchem.2013.11.002.

Williams, P.J., le B., 1998, The balance of plankton respiration and photosynthesis in the open oceans: Nature, v. 394, p. 55–57, https://doi.org/10.1038/27878.

Wu, W., Swanner, E.D., Hao, L., Zeitvogel, F., Obst, M., Pan, Y., and Kappler, A., 2014, Characterization of the physiology and cell-mineral interactions of the marine anoxygenic phototrophic Fe(II) oxidizer *Rhodovulum iodosum*—Implications for Precambrian Fe(II) oxidation: FEMS Microbiology Ecology, v. 88, p. 503–515, https://doi.org/10.1111/1574-6941.12315.

Yee, N., and Fein, J., 2001, Cd adsorption onto bacterial surfaces: A universal adsorption edge?: Geochimica et Cosmochimica Acta, v. 65, p. 2037–2042, https://doi.org/10.1016/S0016-7037(01)00587-7.

Zheng, X.-Y., Beard, B.L., Reddy, T.R., Roden, E.E., and Johnson, C.M., 2016, Abiologic silicon isotope fractionation between aqueous Si and Fe(III)-Si gel in simulated Archean seawater: Implications for Si isotope records in Precambrian sedimentary rocks: Geochimica et Cosmochimica Acta, v. 187, p. 102–122, https://doi.org/10.1016/j.gca.2016.05.012.